Critical Magnetic Scattering in Manganese Fluoride*

M. P. SCHULHOF† AND P. HELLER†
Physics Department, Brandeis University, Waltham, Massachusetts 02154

AND

R. NATHANS
Brookhaven National Laboratory, Upton, New York 11973 and State University of New York at Stony Brook, New York 11790

AND

A. LINZ‡
Center for Materials Science and Engineering, Massachusetts Institute of Technology Cambridge, Massachusetts 02139

(Received 15 September, 1969)

The angular dependence of the quasielastic magnetic scattering has been measured in MnF_2 in the critical region $T>T_N$. The temperature dependence of the inverse correlation range and the staggered mode susceptibility for both transverse and longitudinal spin fluctuations were observed as a function of incident neutron energy over the range $56<E_0<134$ meV. The validity of the quasielastic approximation for this energy region was verified. The data for the longitudinal fluctuations were found to follow simple power laws with the critical exponents $\nu=0.634\pm0.02$, $\gamma=1.24\pm0.02$. An η fitted to the data closest to T_N gave $\eta=0.05\pm0.02$. The transverse fluctuations are not divergent at T_N, although for $T>T_N$ they can be described by power-law fits taken with respect to a temperature $T_\perp\approx66$°K by indices $\nu_\perp=0.63\pm0.08$, $\gamma_\perp=1.47\pm0.1$. The actual critical temperature is $T_N=67.458\pm0.008$.

I. INTRODUCTION

MANGANESE fluoride can be considered as a classical example of a uniaxial antiferromagnetic material. The material has been studied extensively by a variety of experimental techniques.[1,2] Our interest is centered on its behavior near its critical point, in particular the behavior of the spatial dependence of the critical fluctuation above its Néel point. In contrast to neutron experiments on cubic antiferromagnets,[3] $RbMnF_3$, for example, it is possible to separate out the longitudinal and transverse components of the spin fluctuations and to compare their behavior with each other and the equivalent measurements in the cubic cases.

Experimentally, we measure the quasielastic scattering in the neighborhood of the transition point. The interpretation of this scattering in terms of evaluating the staggered susceptibility is straightforward, provided we can establish that the inelasticity in the neutron scattering is not a complicating factor. In particular, we require that the change in wave vector of the scattered neutron due to the inelastic scattering be small compared to the range of the wave vectors over which the scattering is appreciable. This condition is a more stringent one than the usually stated requirement that $E_{\text{inelastic}}\ll E_{\text{incident}}$.

Since the relative momentum transfer in the neutron scattering experiments will depend on the incident neutron wave vector (or energy), we have repeated the measurements for incident neutron energies varying between 56 and 134 meV. As shown in the Appendix, we can estimate the upper limit of the effect of neutron inelasticity on our determinations of κ, the inverse correlation range for different incoming energies. The invariance of our results in the face of the large change in incoming neutron energies, combined with the analysis in the Appendix, strongly suggests that our results do indeed satisfy the quasielastic approximation.

A theoretical calculation given by Moriya,[4] on the basis of a molecular-field assumption, predicts the divergency of the longitudinal staggered susceptibility and corresponding correlation range at the phase transition. The perpendicular susceptibility, however, should remain finite at all temperatures. Our results qualitatively support this prediction, although quantitatively, our results are inconsistent with the molecular-field calculation.

II. THEORY

The theory of neutron scattering by magnetic systems in the critical region was originally given by Van Hove[5] as an extension of the Ornstein-Zernike formulation for simple fluids. The detailed theory has been

* Work performed under the asupices of the U. S. Atomic Energy Commission.
† Supported by U. S. Air Force Grant No. AF 68-1480.
‡ Work supported by Advanced Research Projects Agency Contract No. SD-90.

[1] P. Heller, Phys. Rev. **146**, 403 (1966).
[2] O. W. Dietrich, J. Phys. C. (to be published); M. Antonini, J. Phys. Chem. Solids **28**, 11 (1967); G. Parette, K. U. Deniz, J. Appl. Phys. **39**, 1232 (1968); B. H. Torrie, Proc. Phys. Soc. (London) **89**, 77 (1966); K. C. Turberfield, A. Okazaki, and R. W. H. Stevenson, *ibid.* **85**, 743 (1965).
[3] M. J. Cooper and R. Nathans, J. Appl. Phys. **37**, 1041 (1966); R. Nathans, F. Menzinger, and S. J. Pickart, *ibid.* **39**, 1237 (1968).
[4] T. Moriya, Progr. Theoret. Phys. (Kyoto) **28**, 371 (1962).
[5] L. Van Hove, Phys. Rev. **95**, 249 (1954); **95**, 1374 (1954).

covered in articles by Marshall,[6] deGennes,[7] and Heller.[8]

If the fluctuations in the magnetization occur in a time that is long compared with the transit time of a neutron through a region of correlated spins, and also if the inelasticity is smaller than the magnitude of the thermal fluctuations in the system, then we can relate the angular dependence of the scattering to the wavelength-dependent static susceptibility through the relation

$$\left(\frac{d\sigma}{d\Omega}\right)_{\text{diffuse}}=N\left(1.91\frac{e^2}{mc^2}\right)^2\frac{k_f}{k_i}|F(\mathbf{K})|^2 \times\sum_{\alpha\beta}\{\delta_{\alpha\beta}-\hat{k}_\alpha\hat{k}_\beta\}\frac{k_BT}{g^2\mu_B{}^2}\chi^{\alpha\beta}(\mathbf{K}).$$

$F(\mathbf{K})$ is the ionic form factor normalized to unity at $\mathbf{K}=0$, and α, β refer to the cartesian coordinates of the lattice. The δ function in the curly brackets simply says that we see only those components of the fluctuations perpendicular to the scattering vector $\mathbf{K}$, defined by the incident and final neutron wave vectors $\mathbf{k}_i$ and $\mathbf{k}_f$ through the relation

$$\mathbf{K}=\mathbf{k}_i-\mathbf{k}_f.$$

By looking at a reflection where the spin axis is along the scattering vector, we see only fluctuations perpendicular to the anisotropy axis. When we look at a reflection where the spin axis is at right angles to the scattering vector, we see a known admixture of longitudinal and perpendicular fluctuations. By combining the two results we can find $\chi_{\parallel}(\mathbf{K})$ and $\chi_{\perp}(\mathbf{K})$ separately. From these data, we can evaluate the temperature dependence of the staggered susceptibility $\chi(K=K_0)$ and also determine how χ depends on $\mathbf{K}$; that is, at each temperature we obtain a correlation length for both the parallel and perpendicular components. These data are usually expressed as a function of the distance in reciprocal space corresponding to the change in neutron wave vector.

A. Results for Simple Ornstein-Zernike Theory

For a material with cubic symmetry, χ is a scalar ($\chi_{zz}=\chi_{yy}=\chi_{xx}$), and $\chi(\mathbf{q})$ depends on $|q|$ as

$$\chi(q)=\frac{1}{A(T)}\frac{1}{\kappa_1{}^2+q^2},$$

where $A(T)$ is a slowly varying function of temperature.

This statement is equivalent to saying that the static pair distribution function $G(\mathbf{R})$ is a decaying exponential in R divided by R. In the quasielastic approximation the angular dependence of the scattering is then given by

$$\frac{d\sigma}{d\Omega}=\text{const}\frac{T}{A(T)}\frac{1}{\kappa_1{}^2+q^2}.$$

We expect that the components of χ will be given by

$$\chi_{\parallel}(q,T)=\frac{1}{A_{\parallel}(T)}\frac{1}{\kappa_1(T)^2+q^2},$$

$$\chi_{\perp}(q,T)=\frac{1}{A_{\perp}(T)}\frac{1}{\kappa_{1\perp}(T)^2+q^2}.$$

As we near the critical temperature, $\chi_{\parallel}(0,T)$ will be divergent, with $\chi_{\perp}(0,T)$ remaining finite. In the molecular-field theories describing these phenomena a plot of $1/\chi_{\parallel}(T)$ falls linearly to zero at T_N while a plot of $1/\chi_{\perp}(T)$ extrapolates to zero at a temperature $T_{\perp}<T_N$.

According to a calculation by Moriya[4] for MnF_2, $T_N-T_{\perp}=1.36°K$. Since we do not expect molecular field theory to be valid in the critical region, we shall not assume this value in the analysis of our data. Also, in molecular-field theory we expect that

$$\frac{A_{\parallel}}{A_{\perp}}=\frac{T_N}{T_{\perp}}\cong 1.$$

Again, this was not an explicit assumption in our data analysis.

For a noncubic material such as MnF_2, we expect that the longitudinal and transverse fluctuations will have different temperature dependencies; i.e., χ is a tensor having the tetragonal symmetry of the MnF_2 lattice. We then have to inquire into the form of $\chi^{cc}(T,q)$ and $\chi^{aa}(T,q)$, which we will denote by $\chi_{\parallel}(T,q)$ and $\chi_{\perp}(T,q)$, respectively (a, c denote the crystallographic axes).

Each component of χ will depend on the direction of $\mathbf{q}$ as well as the magnitude. Following Moriya, we shall assume the $\chi(q)$ is constant on ellipsoidal surfaces in q space. That means $\chi(q)$ depends only on the quantity[9]

$$q^*=[q_a{}^2+q_{a'}{}^2+(c/a)^2q_c{}^2]^{1/2}.$$

B. Results for Modified Ornstein-Zernike Theory

Fisher has shown[10] that we may expect deviations from the simple $O-Z$ form close to T_N. This leads to a modification in our expectation for $\chi(q,T)$ as follows:

$$\chi_{\parallel}(q,T)=\left(\frac{1}{A(T)}\frac{1}{\kappa_{1\parallel}(T)^2+q^{*2}}\right)^{1-\eta/2},$$

where η is predicted by Fisher to be a small number for

[6] W. Marshall, R. D. Lowde, Rept. Progr. Phys. **21**, 705 (1968).
[7] P. G. deGennes, in *Magnetism*, edited by G. T. Rado and H. Suhl (Academic Press Inc., New York, 1963).
[8] P. Heller, Rept. Progr. Phys. **30**, 806 (1967).
[9] The physics of q^* can be seen if we imagine that the magnetic fields in the crystal are described by wave vectors. Let $q_{\perp}$ be along the (100) and (010) directions and $q_{\parallel}$ along the (001). Then if a $|q_{\perp}|=c|q_{\parallel}|$, the relative polarizations of neighboring spins will be the same. Thus we would expect $\chi(q_{\parallel})=\chi(q_{\perp})$.
[10] M. E. Fisher, J. Math, Phys. **5**, 944 (1964).

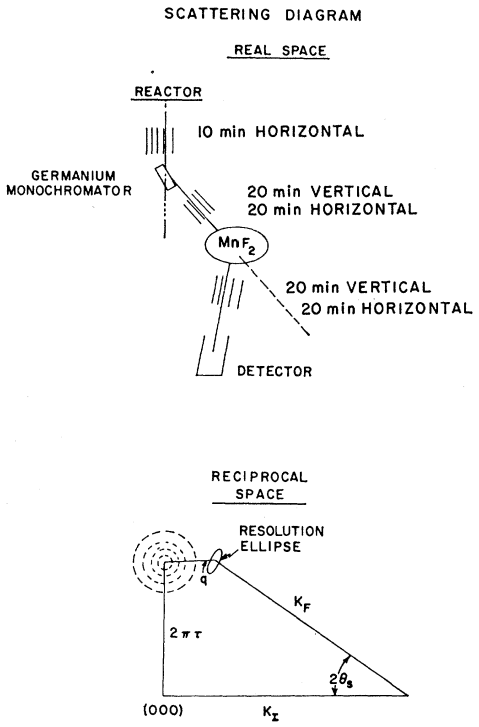

FIG. 1. Diagram of the two-crystal neutron spectrometer. Lower portion gives the equivalent scattering in reciprocal space.

three-dimensional systems. In fact, we find that this modification does give a better fit to the data on the longitudinal fluctuations near T_N. Since the transverse fluctuations do not become singular, this modification is not particularly important, although the data were tested to look for evidence of this effect.

III. EXPERIMENTAL APPARATUS

A. Sample and Spectrometer

Manganese fluoride has a body-centered tetragonal structure (rutile) with the manganese spins ($\frac{5}{2}$) aligned along the c axis in a simple antiferromagnetic manner.[11] The dominant exchange interactions are for next-nearest neighbors ($J_2=-1.76$°K), while nearest neighbors are weakly coupled ($J_1=0.3$°K).[12] The periodicity of the lattice gives a vanishing structure factor for the lowest-order nuclear reflections, so magnetic scattering is observable without an accompanying nuclear peak or the presence of acoustic phonons.

The Néel temperature was determined from a measurement of the disappearance of the magnetic Bragg peak at the (100) reflection. This gave a $T_N=67.465 \pm 0.01$°K, which agrees quite well with the result found from the analysis of the critical scattering above T_N.

[11] The crystal was grown from the melt in a pure helium atmosphere (Czochralski technique) by Dr. D. Gabby and R. Mills. The measured mosaic spread was less than 1-min full width.

[12] G. G. Low, A. Okazaki, R. W. H. Stevenson, and K. C. Turberfield, J. Appl. Phys. **35**, 998 (1964).

Measurements of the critical scattering were made around the (100) and (001) reciprocal points. For the (001) reflection, the spin axis is parallel to the scattering vector, and only transverse fluctuations are observed. For scattering around the (100) reflection, we see a sum of the longitudinal and transverse fluctuations.

The spectrometer is diagrammed in the upper part of Fig. 1. Neutrons from the reactor are monochromated by a deformed germanium crystal. The wave-vector directions are defined by soller slit collimators. Twenty-minute divergences in the horizontal and vertical directions were used before and after the sample. A 10-min horizontal collimator was placed before the monochromator.

B. Temperature Control

Critical scattering measurements require that the sample be maintained at a uniform temperature during the course of the experiment (typically 8 h). For this purpose, the sample was mounted in a controlled-temperature Dewar similar to one used by one of us in an earlier experiment.[3] The actual sample temperature was monitored independently of the servo thermometer by a separate platinum resistance thermometer (PRT) mounted in the base of the sample holder and in good thermal contact with the crystal. This PRT (Leeds and Northrup) was calibrated, using its known resistance at the ice and helium points and using a computer fit to the Z function given by White for interpolation.[13] White estimates that the errors in this process are less than 50 m°K absolute.

The high-gain servo loop used with the control temperature Dewar provided a measured temperature control at the sample crystal of less than ± 0.001 deg over the time of any one measurement. A check for thermal gradients in the crystal was made by masking the incident neutron beam so that only selected portions of the

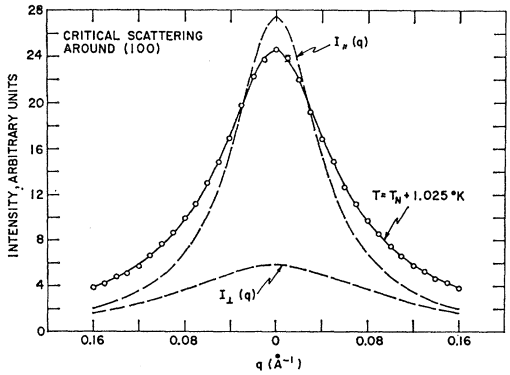

FIG. 2. Critical scattering around the (100) reciprocal lattice point. Experimental points and computer fit (solid line) to data are given. Dashed lines are the separated longitudinal and transverse components.

[13] G. White, *Experimental Techniques in Low-Temperature Physics* (Oxford University Press, New York, 1968), p. 125.

crystal were illuminated and measuring the intensity of a magnetic Bragg peak below T_N (proportional to the square of the magnetization). The agreement between the upper, lower, and bulk crystal at several temperatures (normalized to the lowest temperature) showed that any thermal gradients present were less than (0.002 $\pm$0.003)°K.

C. Resolution Limitations

The resolution limit of the spectrometer can be described as an ellipsoid in reciprocal space where any cross section through the ellipse has a Gaussian intensity profile.[14] If q_x, q_y, q_z define a set of coordinate axes centered around $\mathbf{q}_0$, then the resolution function $R(\mathbf{q}_0)$ describes the probability that a neutron having $\mathbf{q}=\mathbf{q}_0+\mathbf{dq}$ will be counted by the detector. We define

$$R(\mathbf{q}_0)=R_0\exp[-\tfrac{1}{2}(M_{11}q_x^2+M_{12}q_xq_y+M_{22}q_y^2+M_{33}q_z^2)],$$

where M_{ij} are matrix elements that describe the size and orientation of the ellipse.

The actual resolution function was mapped out using the (100) magnetic Bragg peak, and least-square fitted to the form above. The experimental M_{ij}'s were compared with theoretical values calculated from the measured instrumental parameters. The good agreement between the two methods gave confidence that the theoretical resolution function used to correct the data from the (001) reflection (where there is no Bragg peak) was correct.

The experimentally measured data are a convolution of the intrinsic cross section with the instrumental resolution. At temperatures far above T_N the angular distribution is broad and the correction needed small. As $T\rightarrow T_N$ the lines become sharp and the effects due to resolution become quite serious. Corrections to the data were made by folding the resolution function with the the modified Lorentzian cross section given earlier on a point-by-point basis. The parameters in the cross section A, κ_1, η and background were treated as variables in a weighted least-squares fit.

The weighted variance σ^2 was calculated for each set of data, where

$$\sigma^2=\frac{1}{N-M}\sum_i \omega_i[I_i(\text{observed})-I_i(\text{calculated})]^2.$$

Here N is the number of data points, M is the number of free parameters, and counting statistics were used for the weights ω_i. All values of σ^2 were found to vary typically between 0.9 and 1.3. Figure 2 shows data taken at the intermediate wavelength and an intermediate temperature around the (100) reflection, where both components of the fluctuations are seen. The open circles are experimental points, and the solid line is the best fit to the theoretical cross section folded with the instrumental resolution. The upper dashed curve is the corrected cross section for the longitudinal component, and the lower dashed curve is the transverse component.

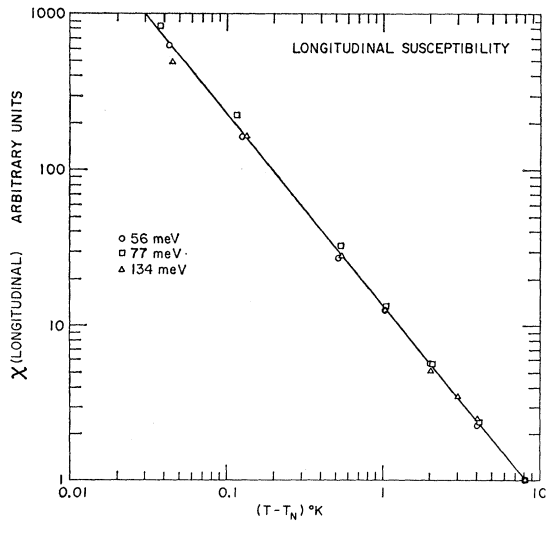

FIG. 3. Longitudinal staggered susceptibility as a function of temperature. Data were taken at three incident neutron energies. Solid line is best fit to a simple power law, in T_N.

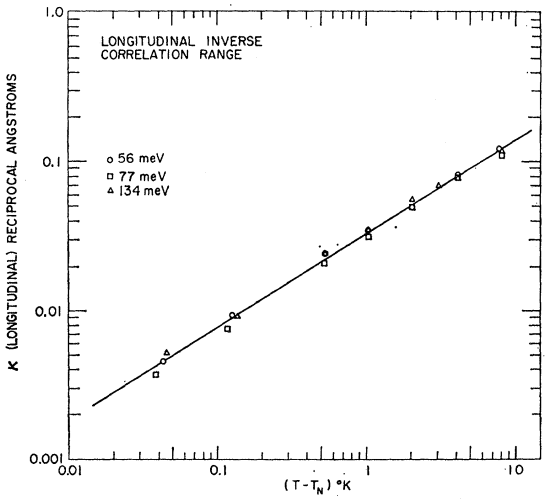

FIG. 4. Longitudinal inverse correlation range. Kappa is in same units as q^*, solid line is best fit to power law in T_N.

IV. RESULTS

Measurements were made in the temperature range T_N+0.04°K to T_N+8°K for incident neutron momenta of 5.2, 6.1, and 8.2 Å^{-1} (56, 77, and 134 meV, respectively). The data taken around the (001) reflection were fitted with a cross section of the form

$$\frac{d\sigma}{d\Omega_{001}}=\left(\frac{B_\perp(T)}{\kappa_{1\perp}^2+q^{*2}}\right)^{1-\eta/2},$$

[14] M. J. Cooper and R. Nathans, Acta Cryst. **A24**, 619 (1968).

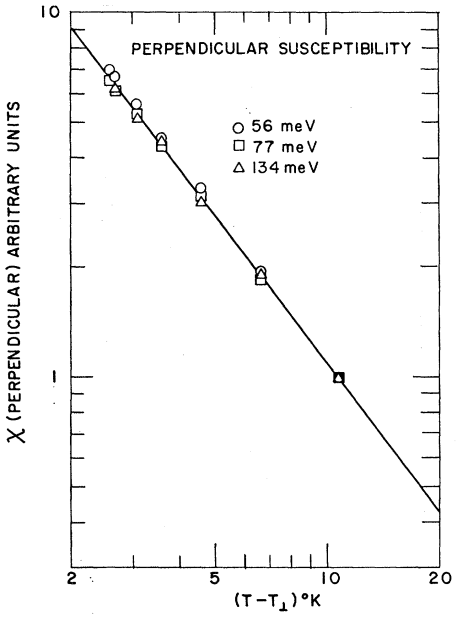

FIG. 5. Transverse staggered susceptibility as a function of $T_\perp$ with best fit to a power law. $T_\perp$ is a parameter of the fit and given in the text.

where B incorporates all of the constant terms given in the complete expression of Sec. II. The data around the (100) reflection were fitted with

$$\left(\frac{d\sigma}{d\Omega}\right)_{100}=\left(\frac{B_{\parallel}(T)}{\kappa_{1\parallel}{}^2+q^{*2}}\right)^{1-\eta/2}+\left(\frac{B_{\perp}'(T)}{\kappa_{1\perp}{}^2+q^{*2}}\right)^{1-\eta/2}.$$

In principle $B_\perp'$ can be calculated from $B_\perp$ and the ratio of the form factors for the (100) and (001) reflections. In practice this is difficult since we cannot guarantee that the neutron illumination remains constant over the crystal when rotating from one reflection to another. The data were analyzed by first fitting the transverse data and finding the value of $T_\perp$ that best described a power-law fit for $\kappa_{1\perp}$. Then $B_\perp'/B_\parallel=T_N/T_\perp\cong 1.05$ was used in the fits to the data from the mixed (100) reflection. This ratio was varied over a 30% range, and it was found that the exponents $\gamma_\parallel$ and $\nu_\parallel$ were unaffected. If $B_\perp'/B_\parallel=2$, then $B_\parallel$ is found to be very temperature-dependent.

The experimental data for the longitudinal susceptibility of the staggered mode are given in Fig. 3. The solid line represents a least-squares fit to the simple power law

$$\chi(q=0)\sim(T-T_N)^{-\gamma},$$

where γ, T_N and the constant of proportionality are all fitted parameters. We find that

$$\gamma=1.238\pm0.02,$$
$$T_N=67.457\pm0.004.$$

Figure 4 shows the corresponding longitudinal inverse correlation length as a function of temperature. κ is in the same units as q^*. The solid line is a fit to a simple power law with respect to T_N:

$$\kappa_{1\parallel}=A\left(\frac{T-T_N}{T_N}\right)^{\nu},$$

where the parameters that best describe the data are given by

$$\nu=0.634\pm0.02,$$
$$T_N=67.459\pm0.007,$$
$$A=0.459\pm0.009=(2.237\pm0.044)/a.$$

The values of T_N found from the data in the critical region agree quite well with the results from the magnetization measurement below ($T_N=67.465\pm0.01$).

It is evident from the data that over the energy range investigated, we do not observe an energy dependence. This result is important if we are to believe that the quasielastic approximation provides a correct description of the scattering observed in this kind of experiment. Given in the Appendix is an estimate of the magnitude of the inelasticities required for us to observe a shift in the data with changing neutron energy.

The sensitivity of the data to an η in the modified Lorentzian cross section was highest in the region closest to T_N. The best value found was

$$\eta=0.05\pm0.02.$$

We also note that the values of γ and ν given above are consistent with the scaling relation

$$\gamma=(2-\eta)\nu$$

for an η equal to 0.047.

These exponents are too large to be consistent with the molecular-field values of

$$\gamma_M=1.0,\quad \nu_M=0.5.$$

However, the magnetization in the region below T_N is known to depart from the molecular field form, and there is no reason why it should be valid above. Fisher and Burford[15] have calculated the critical indices to be expected for an Ising model antiferromagnet with nearest-neighbor interactions on a bcc or sc lattice. They find

$$\gamma=1.25\pm0.007,$$
$$\nu=0.643\pm0.003,$$
$$\eta=0.056\pm0.008,$$

which are close to the values we obtain experimentally, although the model of an Ising system is certainly not valid for manganese fluoride.

Figures 5 and 6 present the measurements of the transverse staggered susceptibility and corresponding correlation range. As expected, these quantities remain finite, although the dependence on temperature in the critical region may be expressed as divergences with

[15] M. E. Fisher and R. Burford, Phys. Rev. 156, 583 (1967).

TABLE I. Results of data analysis at all values of incident neutron energy. Exponents are given for each of the power-law fits described. The combined data represents a fit to all the measured values. η is found from the longitudinal data closest to T_N. Best fit to $\eta=0.05\pm0.02$. Combined data longitudinal values of γ, ν consistent with $\eta=2-\gamma/\nu=0.047$.

Neutron energy (meV)	Experimental results 56	77	134	Combined data
		$\kappa_{1\|\|}=A(T-T_N)^{\nu}$		
ν	0.59 ±0.02	0.65 ±0.01	0.64 ±0.02	0.634 ±0.02
T_N	67.468 ±0.005	67.458 ±0.003	67.450 ±0.008	67.459 ±0.007
A	0.0331±0.0006	0.0306±0.0004	0.0341±0.0008	0.0318±0.0008
		$\chi_{\|\|}(q=0)\sim(T-T_N)^{-\gamma}$		
γ	1.21 ±0.02	1.28 +0.02	1.23 ±0.02	1.24 ±0.02
T_N	67.461 ±0.003	67.455 ±0.003	67.457 ±0.006	67.457 ±0.004
		$\kappa_{1\perp}=B(T-T_\perp)^{\nu}$		
ν	0.65 ±0.1	0.73 ±0.08	0.51 ±0.1	0.63 ±0.08
$T_\perp$	64.87 ±0.7	64.31 ±0.5	65.62 ±0.2	64.92 ±0.7
B	0.028 ±0.008	0.024 ±0.005	0.040 ±0.003	0.0301±0.007
		$\chi_\perp(q=0)\sim(T-T_\perp)^{-\gamma}$		
γ	1.55 ±0.06	1.43 ±0.09	1.41 ±0.09	1.47 ±0.1
$T_\perp$	64.30 ±0.2	64.47 ±0.3	64.49 ±0.3	64.40 ±0.5

respect to a temperature $T_\perp<T_N$. The susceptibility can be fitted to the form

$$\chi_\perp(0)\sim(T-T_\perp)^{-\gamma},$$

and the best fit is found for the values

$$\gamma=1.47\pm0.1,$$
$$T_\perp=64.40\pm0.5.$$

We can also fit the perpendicular inverse correlation range to a power law

$$\kappa_{1\perp}=A\left(\frac{T-T_\perp}{T_\perp}\right)^{\nu}$$

and we find that the best fit is obtained for

$$\nu=0.63\pm0.08,$$
$$T_\perp=64.9\pm0.7,$$
$$A=0.416\pm0.097=(2.028\pm0.47)/a.$$

The average value of $T_N-T_\perp$ found from this method is 2.8 ± 0.8°K, which is different from the one calculated by Moriya from a molecular field theory,

$$T_N-T_\perp{}^M=1.36\text{°K}.$$

If we fit our data, assuming $T_\perp$ given by Moriya, then we do find that the results are described by the classical exponents

$$\nu_m=0.47\pm0.02,$$
$$\gamma_m=0.97\pm0.02.$$

However, the weighted variance goodness of the fit is 50% larger, indicating a poorer fit to the data. Also, the smaller error brackets are hidden in the fact that the number of free parameters has been reduced by 1.

As with the longitudinal data, we find no evidence of a wavelength dependence for the perpendicular spin correlations.

Given in Table I is a summary of the data analysis. The observations at each incident energy were analyzed separately and are presented for comparison with the final values obtained from the combined data.

The error limits quoted for the fitted parameters in each of the power-law fits are the one-standard-deviation points calculated from the least-squares minimum by

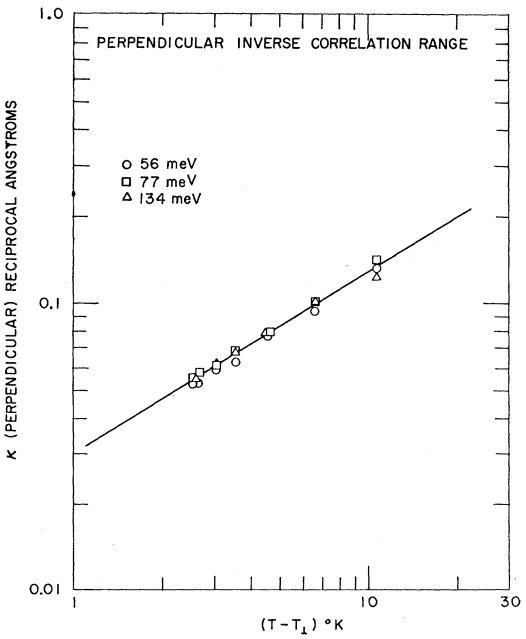

FIG. 6. Transverse inverse correlation range. κ is in the same units as q^*.

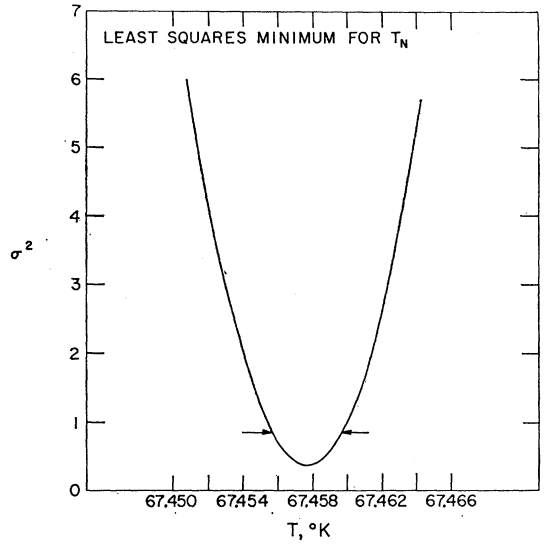

FIG. 7. Least-squares minimum for a typical fit to T_N from the power-law equation for κ (longitudinal). Arrows show the one-standard deviation points calculated by the fitting program.

the fitting program. Figure 7 shows the weighted variance as a function of one of the variable parameters (T_N) for a typical set of data. The equation used in this case was for the fit to the inverse correlation range at an intermediate wavelength. The dip in the minimum corresponds quite well to the errors calculated by the program (shown by the accompanying arrows).

V. CONCLUSIONS

We have made a careful study of the spin fluctuations in manganese fluoride near the critical point

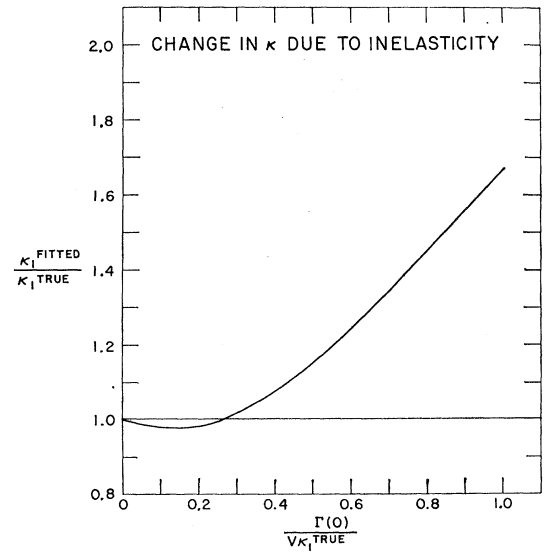

FIG. 8. Changes in κ (fitted) for various inelasticities in the scattering. These results are based on a model for $S(q,\omega)$ given in the Appendix.

($T_N = 67.458 \pm 0.008$°K). The longitudinal staggered susceptibility and corresponding correlation range are found to diverge with critical indices

$$\nu = 0.634 \pm 0.02,$$
$$\gamma = 1.24 \pm 0.02,$$

which are inconsistent with the results predicted from a molecular field theory.

The transverse susceptibility and correlation range remain finite throughout the critical region and may be described as divergences with respect to a temperature $T_\perp < T_N$ by the indices

$$\nu = 0.63 \pm 0.08,$$
$$\gamma_\perp = 1.47 \pm 0.1,$$

where the average value found for $T_N - T_\perp = 2.8 \pm 0.8$°K is greater than the result given by Moriya from a molecular field calculation (1.36°K).

The correctness of the data interpretation within the context of the quasielastic approximation has been experimentally verified for the range of incident neutron energies 56–134 meV. The data were analyzed by correcting for instrumental resolution and fitting to a modified Ornstein-Zernike cross section. The parameter η defined by Fisher to describe the departure from Lorentzian behavior is found to have a value

$$\eta = 0.05 \pm 0.02$$

in the region close to T_N.

The results given here are to be compared with those of Dietrich,[2] who has made recent measurements of the neutron inelastic scattering in MnF_2 for small momentum transfers. He analyzed his data using an assumed analytic form for the inelastic cross section. Although the direct measurement of inelastic cross section gives a somewhat more direct measurement of the same parameters we have evaluated here, the statistical accuracy of the data is much less than that which can be obtained in the two-axis arrangement used in our work. The choice is one of evaluating all the parameters connected with the critical scattering from the somewhat poorer data associated with inelastic neutron work. This procedure requires fewer assumptions on the presumed analytical form of the cross section. Alternatively, we may choose to collect data of greater statistical accuracy and verify the approximations used in interpretation of the data, a procedure we have used here. As a whole, there is satisfactory agreement between our results and those of Dietrich. Small differences are evident, particularly with regard to the absolute values of κ. The explanation of these differences is not immediately obvious. The complexity of the analysis in the least-square analysis involving multiple parameter evaluations tends to obscure the interactions between analysis and accuracy of data.

We are now in the process of analyzing our own inelastic results with a view to examining these small discrepancies.

ACKNOWLEDGMENTS

We wish to thank Dr. J. M. Hastings, Dr. L. M. Corliss, and Dr. H. Lau for helpful information about experimental techniques. Credit is also due to Dr. M. Blume, Dr. G. Shirane, and Dr. M. Fisher for fruitful discussions.

APPENDIX: AN ESTIMATE OF EFFECTS OF INELASTICITY

On the basis of some simple assumptions about the nature of the scattering function $S(q,\omega)$ we can estimate what magnitude of inelasticity would have to be present for us to see a shift in the value of κ we fit to our data as the incident neutron energy is varied.

We consider only the longitudinal fluctuations and neglect the effects of the Boltzmann factor, which is valid if $\hbar\omega \ll k_B T$. The scattering function can be written as a function of q and ω:

$$S(q,\omega)=A(q)/[\omega^2+\Gamma(q)^2],$$

where $\Gamma(q)$ is the energy width due to inelasticity as a function of q, and $A(q)$ can be found by relating the integral of $S(q,\omega)$ over energy to the static form of the cross section.

$$\int S(q,\omega)d\omega=B(T)/[\kappa_1^2(T)+q^2],$$

so we find that

$$A(q)=\frac{B(T)}{\kappa_1^2+q^2}\frac{\Gamma(q)}{\pi},$$

and we can now write

$$S(q,\omega)=\frac{1}{\pi}\frac{B(T)}{\kappa_1^2+q^2}\frac{\Gamma(q)}{\omega^2+\Gamma(q)^2}.$$

The exact form for $\Gamma(q)$ is not known; however, a reasonable assumption is to adopt the scaling relation

$$\Gamma(q)=\Gamma(0)(1+q^2/\kappa_1^2).$$

If we use this form in the equation above for $S(q,\omega)$ we get that

$$S(q,\omega)=\frac{B}{\kappa_1^2}\Gamma(0)\frac{1}{\omega^2+\Gamma(0)^2(1+q^2/\kappa_1^2)^2}.$$

In order to relate the static susceptibility we actually measure to the integral of $S(q,\omega)$, we have to ask what range of q is observed when the spectrometer is set to q_0. This is not related to the resolution function (although that also smears out the q value), but is a property of the fact that the two-crystal apparatus counts any neutron that exists along the direction of final momentum defined by the counter. Any inelasticity present will produce a shift in the q we actually measure. We can write down the q as a function of energy

$$q(\omega)^2=q_0^2+(\omega/V)^2-2q_0(\omega/V)\cos\alpha,$$

where α is the angle q_0 makes with k_{final}, and V is the neutron velocity.

The static susceptibility measured as a function of q_0 is then

$$\chi(q_0)=\int S(q(\omega),\omega)d\omega.$$

This can be reduced to a dimensionless form and integrated numerically for fixed values of $\Gamma(0)$. We may then ask what the result is of fitting the generated $\chi(q_0)$ to the simple Lorentzian cross section for various values of the inelasticity. This procedure will show how the fitted values of κ vary as a function of inelasticity. In the limit of infinite neutron velocity the fitted κ must equal the true κ exactly.

In Fig. 8 we have plotted the behavior of κ fitted as a function of the inelasticity. The scales are in dimensionless units. We may now ask what inelasticity would have to be present for us to see a shift in the κ's we observed over the variation in neutron energy measured. From the accuracy of our data, a 15% change would be easily detected. This corresponds to a dimensionless inelasticity of 0.5. Using the actual κ's observed implies a $\Gamma(0)$ of 1 meV at a temperature 6°K above the Néel point. Closer in, say 0.15° above, a $\Gamma(0)=0.1$ meV would be required to produce the same shift in κ.

From the figure, we can see why the quasielastic approximation is not valid at lower energies. If we decrease the neutrong energy by a factor of 4 then the inelasticity increases by a factor of 2, and the shift in κ can become serious.